Semiconductors, Vol. 38, No. 10, 2004, pp. 1225–1229. Translated from Fizika i Tekhnika Poluprovodnikov, Vol. 38, No. 10, 2004, pp. 1265–1269.

PHYSICS OF SEMICONDUCTOR DEVICES

Ge/Si Waveguide Photodiodes with Built-In Layers of Ge Quantum Dots for Fiber-Optic Communication Lines

A. I. Yakimov^, A. V. Dvurechenskiĭ, V. V. Kirienko, N. P. Stepina, A. I. Nikiforov, V. V. Ul'yanov, S. V. Chaĭkovskiĭ, V. A. Volodin, M. D. Efremov, M. S. Seksenbaev, T. S. Shamirzaev, and K. S. Zhuravlev

Institute of Semiconductor Physics, Siberian Division, Russian Academy of Sciences, pr. Akademika Lavrent'eva 13, Novosibirsk, 630090 Russia

^e-mail: yakimov@isp.nsc.ru

Submitted February 3, 2004; accepted for publication February 11, 2004

Abstract—The results of research aimed at the development of high-efficiency Ge/Si-based photodetectors for fiber-optic communication applications are reported. The photodetectors are designed as vertical *p–i–n* diodes on silicon-on-insulator substrates in combination with waveguide lateral geometry and contain Ge quantum-dot layers. The layer density of quantum dots is 1×10^{12} cm^{-2}; the dot size in the plane of growth is ~8 nm. Unprecedentedly high quantum efficiency suitable for the range of telecommunication wavelengths is attained; specifically, in the waveguides illuminated from the end side, the efficiency was as high as 21 and 16% at 1.3 and 1.55 μm, respectively. © *2004 MAIK "Nauka/Interperiodica".*

1. INTRODUCTION

One of the most important areas in the development of information transfer facilities in television and telephone networks, the Internet, and optical computers is the elaboration of fiber-optic communication lines (FOCLs). FOCLs contain a transmitter and a receiver, commutation elements, and fiber-optic waveguides. In the transmitter, electrical signals pass an electron control circuit and enter a semiconductor radiator (a laser or a light-emitting diode), where they are converted into optical signals that are fed via matching devices into a fiber-optic waveguide and propagate there to a specified point. A photodetector (PD) detects the radiation and performs the optoelectrical conversion and the subsequent amplification of the electrical signals.

Quartz is conventionally employed for optical waveguides incorporated in FOCLs. An absorption spectrum of high purity quartz typically features three windows of transparency in the vicinity of 0.85, 1.3, and 1.55 μm. This region also corresponds to the nearest atmospheric transparency window. It is currently assumed that the near-infrared (IR) range from 1.3 to 1.55 μm is the most appropriate for FOCL applications.

The wide use of FOCLs is hindered by the high cost of optical transmitter–receivers operating in the near-IR spectral region. It is expected that the implementation of a silicon-compatible technology for the production of photonic FOCL elements will significantly reduce the cost of such elements and allow monolithic integration of all components including radio-amplifying and shifting electronics on the basis of a simple, reliable, and easy-to-reproduce optoelectronic integrated circuit [1]. However, silicon itself is transparent for radiation with a wavelength larger than 1.1 μm. A fairly high sensitivity in the vicinity of the wavelength $\lambda \approx 1.5$ μm can be obtained with germanium PDs. This circumstance means that researchers are currently interested in developing Ge/Si heterostructures that are sensitive at room temperature within the telecommunication wavelength range from 1.3 to 1.55 μm.

As for the prospects for incorporating Ge/Si heterojunctions into the concept of silicon VLSI, Ge/Si heterostructures with coherently introduced Ge nanoclusters (quantum dots) are the most promising, since these structures offer the possibility of overgrowing the elastically stressed germanium layers with well-structured Si layers, which may serve as a base for the subsequent VLSI elements to be mounted on. Furthermore, such a system has already been employed in light-emitting diodes radiating at room temperature in the range 1.3–1.55 μm with the quantum yield at a level of 0.015% [2].

Initially, Ge/Si photodiodes with Ge quantum dots (QDs) were designed for normal incidence of light on the side of the *p–n* junction plane [3, 4]. The quantum efficiency η ranged from 3 to 8% for $\lambda = 1.3$–1.46 μm. One can increase the quantum efficiency by using a waveguide structure that involves the effect of multiple internal reflection from the walls of the waveguide. Since the optical beams should propagate in the plane of the integrated circuit, which includes all the necessary FOCL elements [1], such a design is advantageously suited to end-on illumination of the detector. The fabrication of waveguide photodetectors based on Ge/Si heterostructures with coherently introduced Ge nanoislands was reported in [5, 6]. The highest quantum efficiency attained at the wavelength $\lambda = 1.3$ μm

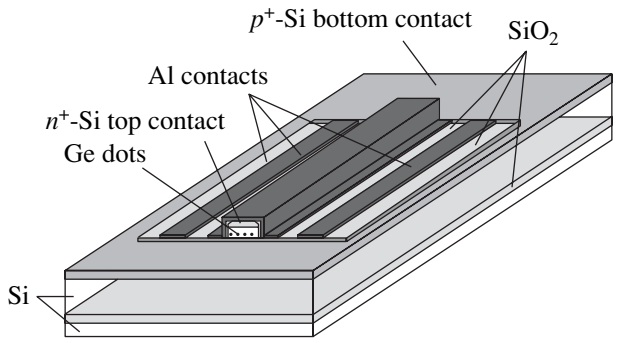

Fig. 1. Schematic representation of the photodetector formed on a silicon-on-insulator substrate.

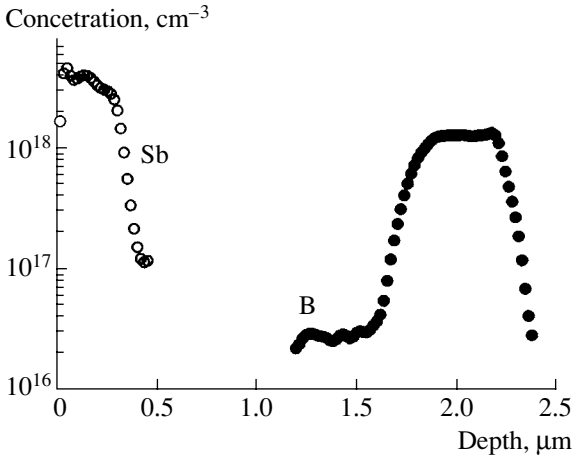

Fig. 2. SIMS profiles of boron and antinomy concentrations across the epitaxial layer starting from the surface.

was $\eta = 5.3$ and 9.5% for a PD structure in the form of a *p–i–n* diode [5] and a bipolar *n–p–n* phototransistor [6], respectively. It should be noted that in [5, 6] the layer density of islands was 1×10^{11} cm^{-2} or lower. Clearly, one way to further increase the quantum efficiency of photoconversion in such structures is to raise the density of Ge nanoclusters. The aim of this study is to develop a waveguide Ge/Si photodetector containing arrays of Ge QDs with a layer density at 10^{12} cm^{-2} and featuring high sensitivity over the telecommunication wavelength range.

2. PHOTODETECTOR PRODUCTION TECHNOLOGY

The photodetectors under study were silicon *p–i–n* diodes with 36 layers of Ge islands built into the base region that were divided by 30-nm-wide Si layers. Each device combined a vertical photodiode and lateral waveguide (Fig. 1). In order to obtain high-density germanium islands, they were formed by molecular-beam epitaxy (MBE) in the Volmer–Weber growth mode on a preliminarily oxidized silicon surface [7]. In our previous studies, it was shown that this procedure allows one to yield layers of Ge nanoclusters that are coherently matched to Si and have a layer density of up to 10^{12} cm^{-2} for sizes no larger than 10 nm [4, 7, 8].

As substrates, we used the silicon-on-insulator (SOI) wafers fabricated by SMART CUT technology (Wafer World, Inc.). The silicon layer cut off from the SOI structure and the buried oxide had thicknesses of 280 nm and 380 nm, respectively. The upper silicon layer was (100)-oriented. Before the MBE process, the silicon layer was thinned to 250 nm by thermal oxidation with subsequent etching of the oxide in a hydrofluoric acid solution. The diffraction pattern obtained from the silicon surface indicated that the SOI-wafer working layer was of high crystal quality and would be suitable for epitaxial growth. In the near-IR region, the difference between the Si and SiO_2 refractive indices is equal to two, which is sufficiently high to allow efficient spatial focusing of a beam propagating in the waveguide over the substrate plane.

Both the Si and Ge layers were grown at 500°C. The growth rate was maintained at a level of 0.3 and 0.03 nm/s for Si and Ge, respectively. At first, after the conventional cleaning of the SOI surface, a 500-nm-thick p^+-Si layer doped with boron to a concentration of 1×10^{18} cm^{-3} was grown; then, a 100-nm-thick buffer layer of nominally undoped Si was deposited. After that, oxygen was let into the growth chamber and the Si surface was oxidized for 10 min at an oxygen pressure of 10^{-4} Pa and a substrate temperature of 500°C. This procedure resulted in the formation of a SiO_x layer with a thickness of several angstroms. Oxygen was then pumped out of the chamber so that the pressure decreased to 10^{-7} Pa and a 0.5-nm-thick Ge layer was deposited and overgrown with Si to a thickness of 30 nm. The overgrowth was preceded by an increase in the wafer temperature to 600°C over a short period (2 min). Such annealing was necessary for the subsequent growth of defect-free Ge layers. The last four procedures (oxidation, the deposition of a 0.5-nm-thick Ge layer, annealing for 2 min, and the deposition of a 20-nm-thick Si layer) were successively repeated 36 times. The resulting multilayer Ge/Si structure was covered with a 100-nm-thick Si layer. The background concentration of boron in the nominally undoped Si layers was 3×10^{16} cm^{-3}. Finally, the formation of the *p–i–n* diode was completed by the growth of a 300-nm-thick n^+-Si layer (with an Sb concentration of 4×10^{18} cm^{-3}). Figure 2 shows the boron and antimony concentration profiles in the structure according to the data of secondary-ion mass spectrometry.

The state of the grown Ge layer surface was checked using scanning tunneling microscopy (STM). By statistical processing of the surface profiles, the average size of the Ge islands in the growth plane was estimated as ~8 nm, and the density of islands, ~10^{12} cm^{-2}. Reference specimens on silicon substrate–satellites were grown for Raman scattering (RS) and photoluminescence (PL) measurements. The sequence of layers was

the same as in the SOI wafers, except for the upper n^+-Si layer, which was absent in the reference structures. Also, the number of Ge layers in the reference structures was only 10 instead of 36.

The fabrication of PDs was continued on a silicon linear array using a specially designed set of photomasks. The waveguide width was 50 μm and the length varied from 100 μm to 5 mm. The vertical walls were formed by the conventional photolithography method and plasma–chemical etching to a depth of 1.6 μm. The buried SiO_2 layer was used as a reflective coating on the substrate side, while a 70-nm-thick aluminum foil was used for the same purpose on the lateral walls of the waveguide, where it also served as an electrical contact to the upper n^+-Si layer. The illuminated end face of the waveguide, like all the other walls, was covered with a 225-nm-thick pyrolytic SiO_2 layer, which also functioned as an antireflection layer at wavelength of 1.3 μm.

3. RAMAN SCATTERING

We analyzed the structure of Ge nanoclusters using the data of Raman scattering (RS) spectroscopy. The RS spectra of the structures under excitation by Ar-laser radiation ($\lambda = 514.5$ nm) were detected at room temperature using a computer-controlled setup built around a DFS-52 spectrometer (LOMO, St. Petersburg) in the quasi-backscattering geometry. We used the polarization scattering geometry *XY*; i.e., the incident radiation was polarized along the crystallographic direction [001] (*X* axis) and the scattered radiation was detected in the polarization [010] (*Y* axis). This geometry was chosen since it is allowed for scattering by LO phonons in Ge and Si and is forbidden for two-phonon scattering by TA phonons from the silicon substrate. Thus, we avoided the difficulties encountered during the interpretation of RS spectra in [9].

Figure 3 shows the Raman spectra of a sample with Ge islands and a Si substrate in *XY* geometry and the spectrum obtained from the silicon substrate without the polarization analysis of the scattered light. The latter spectrum shows peaks that correspond to two-phonon RS by TA phonons of silicon and are similar to those observed in [9]. It can be seen that, in *XY* polarization geometry, these peaks have another shape and have an intensity that is more than one order of magnitude lower (for clarity and ease of comparison, the spectrum in *XY* geometry from the Si substrate is multiplied by a factor of 10). The spectrum of the sample with Ge nanoclusters contains peaks that correspond to RS by optical vibrations of Ge–Ge and Ge–Si bonds, as well as by optical vibrations of Si–Si bonds (from the substrate). Analysis of the position and intensity of the RS spectrum allowed us to estimate the stoichiometry level and the stresses in the Ge islands.

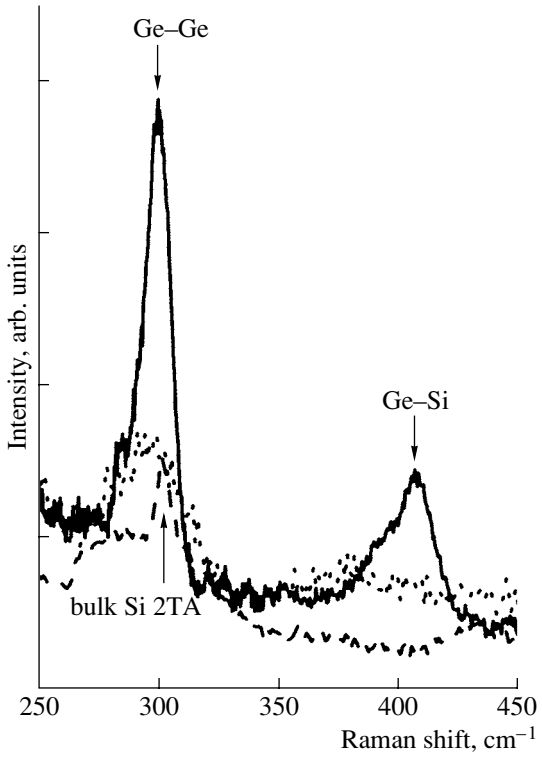

Fig. 3. Raman spectra (solid line) in a sample with Ge nanoclusters and (dotted line, with intensity multiplied by a factor of 10) in the Si substrate in *XY* geometry. The dashed line shows the spectrum from the silicon substrate without polarization analysis of the scattered light.

The integrated intensities of scattering by Ge–Ge and Ge–Si bonds are related as

$$\frac{I_{\mathrm{GeGe}}}{I_{\mathrm{SiGe}}} \approx B\frac{x}{2(1-x)}, \qquad (1)$$

where $B = 3.2$ [10]. Based on these data, we established the relative content of germanium in the islands x within the range 0.65–0.70.

We analyzed the position of the RS peaks using the approach described in [11, 12]. Since the optical-phonon frequency at the center of the Brillouin zone for bulk germanium equals 302 cm^{-1}, the frequencies of Si–Si, Ge–Si, and Ge–Ge bonds can be approximated as

$$\begin{aligned}\omega_{\mathrm{SiSi}} &= 520.5 - 62x - 8.15\varepsilon,\\ \omega_{\mathrm{GeSi}} &= 400.5 + 14.2x - 5.75\varepsilon,\\ \omega_{\mathrm{GeGe}} &= 302 - 18(1-x) - 3.85\varepsilon, \qquad (2)\end{aligned}$$

where x is the Ge content in the islands and ε is the relative mismatch of the lattice constants. In [12] the values of these frequencies (in cm^{-1}) are presented versus the composition (when x does not exceed 0.4) and the relative mismatch of the lattice constants in the plane of growth (100) ε (in percent). The shift is taken for Ge and is negative in the case of compression. Expressions (2)

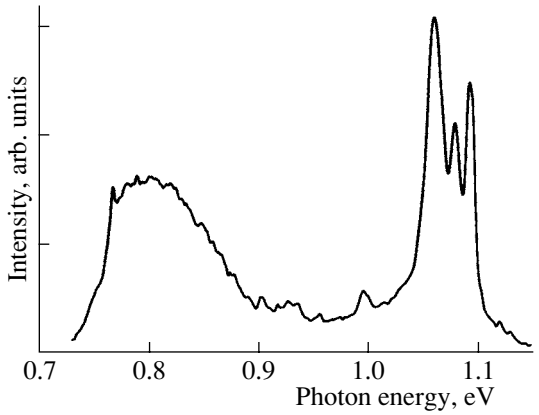

Fig. 4. PL spectrum measured at 4.2 K.

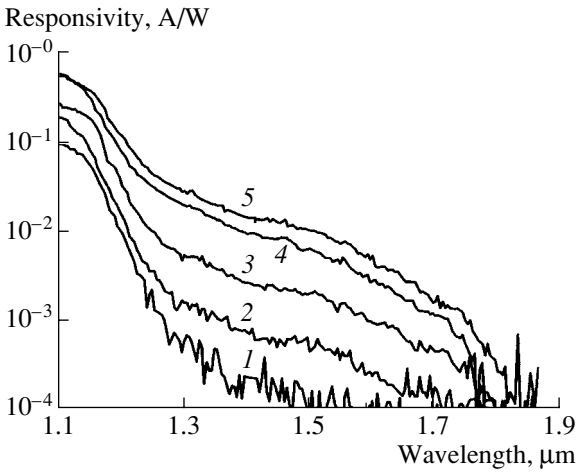

Fig. 5. Sensitivity spectra of the photodetectors with different waveguide length L in short-circuit mode: L = (*1*) 0.2, (*2*) 0.5, (*3*) 1, (*4*) 2, and (*5*) 3 mm; room-temperature measurements.

extrapolate these dependences to the region of nanoclusters with the Ge content x approaching unity.

The maximum signal from Ge–Ge bonds is observed at 300 cm^{-1} (Fig. 3). Taking into account that, because of the size-related quantum effect, the peak for 1.4-nm-high islands is shifted to lower frequencies by 4 cm^{-1}, we can evaluate its position in unstrained $Ge_{0.7}Si_{0.3}$ nanoclusters at 292.5 cm^{-1}. Thus, the total shift due to stresses equals 7.5 cm^{-1}. The maximum relative difference between the lattice constants in completely strained nonrelaxed $Ge_{0.7}Si_{0.3}$ islands and the Si matrix is 2.9%. Hence, it follows that the maximal shift of the RS peak due to stress in nonrelaxed islands would equal 11 cm^{-1}. This result means that the relaxation of stresses in germanium nanoclusters amounts to 30%.

4. PHOTOLUMINESCENCE

The steady-state photoluminescence (PL) spectra were measured using a setup based on an SDL-1 double monochromator with a 300 groove/mm grating (focal distance, 600 mm). The PL was excited using Ar-laser radiation (λ = 488 nm) with a power density of 25 W/cm^2. Emission was detected using a liquid-nitrogen-cooled germanium *p–i–n* photodiode (Edinburgh Instruments). Figure 4 shows the PL spectrum measured at 4.2 K. The spectrum features a set of lines in the range 1.05–1.1 eV that correspond to the exciton recombination in silicon and a broad band in the vicinity of 0.8 eV (λ = 1.55 μm) attributed to indirect (in real space) optical recombination between holes localized in Ge islands and electrons at the type-II heteroboundary in Si. The low-energy edge of the PL signal from the islands is defined by the edge of the Ge-detector spectral characteristic. The presence of efficient PL in the wavelength range of interest allows one to hope that waveguide photodetectors will provide highly efficient photoconversion.

5. PHOTOELECTRIC CHARACTERISTICS OF THE PHOTODETECTOR

Typical spectral dependences of the current–power sensitivity of the photodetector in the short-circuit mode (bias U = 0) when the waveguide ends are illuminated are shown in Fig. 5. Different curves correspond to different waveguide lengths L. The photoresponse of the samples was measured at room temperature using an IKS-31 infrared spectrometer and a phase-sensitive nanovoltmeter at a modulation frequency of 560 Hz. The spectral characteristics of illuminance were obtained using a cooled CdHgTe photoresistor. In order to exclude the penetration of light into the substrate, which would lead to an erroneous value of illuminance because of an increase in the area that is illuminated in reality, the light beam was directed onto the detector from above at an angle of ~5° relative to the normal to the detector's end face. As for the photosensitive area, we took the value 50 × 400 μm^2, where 50 μm is the waveguide width and 400 μm is the total thickness of the structure including the substrate. This procedure disregards the optical coupling of light in the waveguide and yields the lower-bound estimate of the sensitivity and quantum efficiency.

Figure 6 shows the dependences of quantum efficiency η at the wavelengths λ = 1.3 and 1.55 μm on the waveguide length and the reverse bias. The values of η were calculated from the relationship between the sensitivity R, photon energy $h\nu$, and the elementary charge e: $R = (rh\nu)\eta$. It turned out that the maximum quantum efficiency is attained in the structures with waveguide length L > 3 mm (Fig. 6a) at reverse bias U > 3 V (Fig. 6b) and is as high as 21 and 16% for wavelengths of 1.3 and 1.55 μm, respectively. The flattening out of η observed in long waveguides apparently indicates that the light that penetrates the face of the edge and propagates over the germanium layers is completely absorbed in this case. We previously observed the flattening of the photoresponse with reverse bias in the

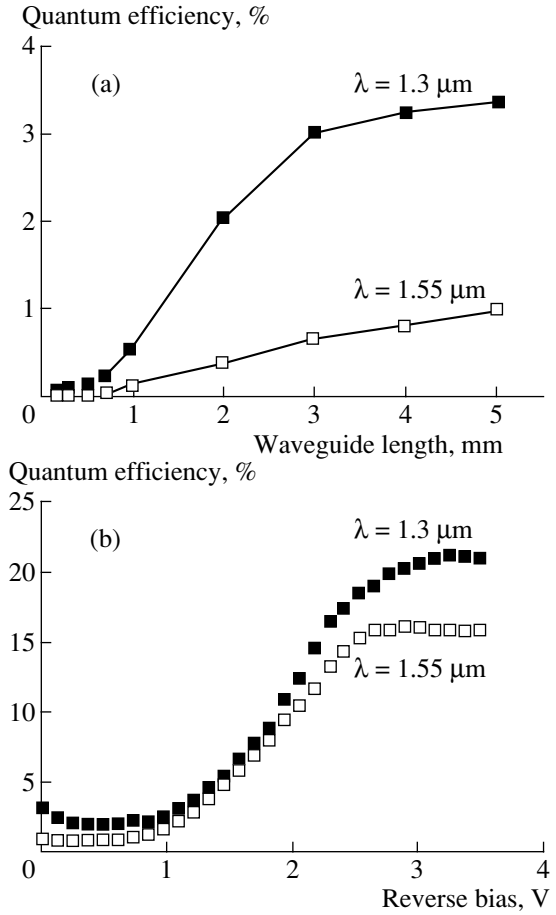

Fig. 6. Quantum efficiency at 1.3 and 1.55 μm vs. (a) the waveguide length in short-circuit mode and (b) the reverse bias for the waveguide length $L = 4$ mm.

conventional geometry of Ge/Si-based *p–i–n* photodiodes whose *p–n* junction side was illuminated [4]; we attributed this effect to the electric-field stimulation of ejection of photoholes localized in Ge islands into the valence band.

6. CONCLUSIONS

The main results of this study can be formulated as follows:

(i) A method for the production of waveguide silicon *p–i–n* photodiodes with built-in layers of Ge quantum dots on silicon-on-insulator substrates for the telecommunication wavelength range (1.3–1.55 μm) is developed. The layer density of quantum dots is 10^{12} cm^{-2}, and the dot size does not exceed 10 nm.

(ii) Due to both the effect of multiple internal reflection and the high density of Ge nanoclusters in the active region, we obtain a quantum efficiency of 21 and 16% at wavelengths of 1.3 and 1.55 μm, respectively.

ACKNOWLEDGMENTS

This study was supported by the Russian president's program for Young Doctors of Science (project no. MD-28.2003.02) and INTAS (grant no. 2001-0615).

REFERENCES

1. H. Presting, Thin Solid Films **321**, 186 (1998).
2. W.-H. Chang, A. T. Chou, W. Y. Chen, *et al.*, Appl. Phys. Lett. **83**, 2958 (2003).
3. S. Tong, J. L. Wan, and K. Wang, Appl. Phys. Lett. **80**, 1189 (2002).
4. A. I. Yakimov, A. V. Dvurechenskiĭ, A. I. Nikiforov, *et al.*, Fiz. Tekh. Poluprovodn. (St. Petersburg) **37**, 1383 (2003) [Semiconductors **37**, 1345 (2003)].
5. M. Elcurdi, P. Boucaud, S. Sauvage, *et al.*, Physica E (Amsterdam) **16**, 523 (2003).
6. A. Elfving, G. V. Hansson, and W.-X. Ni, Physica E (Amsterdam) **16**, 528 (2003).
7. A. I. Nikiforov, V. V. Ul'yanov, O. P. Pchelyakov, *et al.*, Fiz. Tverd. Tela (St. Petersburg) **46**, 80 (2004) [Phys. Solid State **46**, 77 (2004)].
8. A. I. Yakimov, A. V. Dvurechenskii, A. I. Nikiforov, *et al.*, Phys. Rev. B **67**, 125318 (2003).
9. A. V. Kolobov, J. Appl. Phys. **87**, 2926 (2000).
10. P. M. Mooney, F. Dacol, J. C. Tsang, and J. O. Chu, Appl. Phys. Lett. **62**, 2069 (1993).
11. F. Cerdeira, C. J. Buchenauer, F. H. Pollak, and M. Cardona, Phys. Rev. B **5**, 580 (1972).
12. J. Groenen, R. Carles, S. Christiansen, *et al.*, Appl. Phys. Lett. **71**, 3856 (1997).

Translated by A. Sidorova-Biryukova